Study of Pulsed RF Signal Extraction and Irradiation from a Capacitive Nonlinear Transmission Line

Leandro C. Silva[1], José O. Rossi[1], Elizete G. L. Rangel[1], Lucas R. Raimundi[1], Edl Schamiloglu[2]

[1]National Institute for Space Research, INPE, Brazil
Email: leandro@lit.inpe.br
[2] University of New Mexico, UNM, USA
Email: edls@unm.edu

Abstract—Research on Nonlinear Transmission Lines (NLTLs) has long been carried out to produce oscillating pulses. The radiofrequency (RF) pulses generated by the NLTLs can be radiated by antennas connected to the output of the lines. Possible applications of NLTLs as an RF generator include aerospace radars, telecommunications, battlefield communication disruption, and medical devices. There have been relatively few articles that presented experimental results regarding the extraction and the radiation of the RF signal from NLTLs. This article reports the excellent results obtained with a low voltage lumped capacitive NLTL in which oscillations of the order of 230 MHz were produced and radiated using Double-Ridged Guide (DRG) antennas. The RF signal was extracted using a decoupling circuit based on a Chebyshev high-pass filter. The NLTL was evaluated through time domain and frequency domain analyses of the pulsed RF signal measured on a resistive load connected to the output of the line, as well as on transmitting and receiving by antennas. The LT-SPICE model of the line was implemented and the comparison of simulation and experimental results presented a good agreement.
Keywords— Nonlinear transmission lines (NLTLs), RF radiation, varactor diode, filter.

I. INTRODUCTION

Recently, the NLTL technology has been studied to produce high power microwave signals. The NLTLs can be used as an alternative technique for pulsed high-power transmitters that includes the RF generator and the solid state (SSA) / traveling wave tube (TWT) amplifiers [1,2]. High power pulses with a peak power of 20 MW have been produced in the frequency range of 1 GHz [3]. In [4], a capacitive NLTL produced a peak power of 60 MW at 200 MHz. Other works presented the development of high power NLTLs for medical applications [5,6]. They are studying the physiological responses of pulsed RF signal focusing on cancer treatment. Another study demonstrated the design of Radiofrequency Identification (RFID) system based on NLTL [7]. RFID uses electromagnetic fields to identify and track tags attached to objects. It is often seen as an important component of the Internet of Things (IoT) [8].

The high power NLTL could be used as a transmitter section of aerospace radars that includes the pulse modulator and the high power amplifier. In a pulsed radar, the transmitted RF pulsed signal reflects from a surface of an object and returns to a receiver giving information about the location and the speed of the object. Signal processing of this information can be used to create a high-resolution image of the object. This technology is used in Synthetic Aperture Radar (SAR) [9].

A recent article presented the advances that have enabled CubeSats as viable platforms for radar missions. However, the size and weight constraints of the CubeSat drive many of the radar RF design challenges [10].

Considering that the NLTLs used as a pulsed RF transmitter offer advantages such as simplicity, lightweight, compactness and lower cost, this technology can be seen as a promising alternative for space missions involving nanosatellites.

Very few articles presented experimental results regarding the transmission and reception of the RF signals generated by lumped capacitive NLTLs.

Although most of the studies are concentrated on high voltage NLTL, an experiment with low voltage has the advantage that the NLTL can be assembled with commercial-off-the-shelf (COTS) components and the measurements can be performed with good accuracy in the laboratory. This kind of experiment is important to evaluate the soliton propagation characteristics such as time delay, width, number of oscillations and voltage

modulation depth (VMD).

Previous works investigated the performance of low voltage capacitive NLTLs. They analyzed the nonlinear partial differential equation (PDE) of these networks, the influence of the input pulse shape and the resistive load on the RF generation [11-13].

This paper reports an investigation of the performance of a 20-section lumped capacitive NLTL based on varactor diodes. In this work, the line was driven by a 13 V input signal with a frequency repetition rate of 5 MHz to produce a pulsed RF signal with oscillations of voltage modulation depth (VMD) of about 5 V and frequency around 230 MHz.

The pulsed signal generated by the NLTL was first measured on a resistive load. Then a Chebyshev filter was designed and connected to the line output to extract only the high-frequency spectral components of the signal.

The output signal was radiated and received using two double-ridge guide antennas. The NLTL performance was evaluated through time domain analysis and Fast Fourier transform (FFT) of the RF signal. An LT-SPICE model of this line was used for comparison between simulations results and experimental data.

II. NLTL BASIC THEORY

A capacitive NLTL is implemented using inductors and variable capacitors as nonlinear components arranged in a series of LC section low pass filters (Fig.1). In this experiment, a varactor diode is used as a variable capacitor (Fig. 1). The capacitance of the diode varies according to the applied reverse voltage.
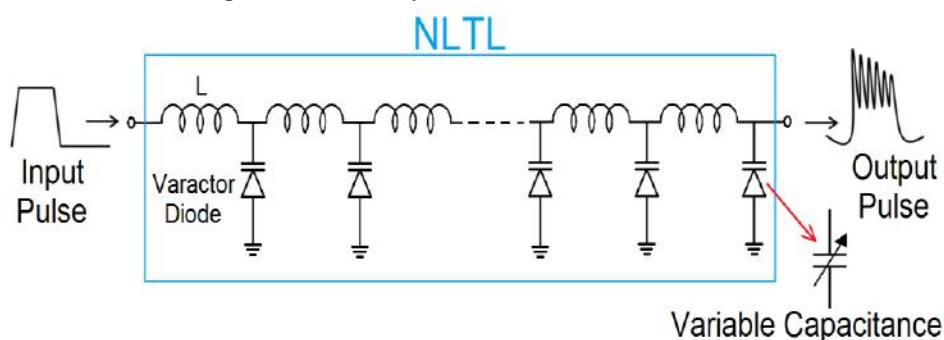

Fig. 1: NLTL circuit using varactor diodes as variable capacitors.

The input pulse injected into the line propagates down the line length. As the capacitance of the varactor diodes decreases with the pulse amplitude, the portion of the pulse with higher amplitude will travel faster than its part with lower amplitude. It happens because the propagation velocity of the pulse increases as the voltage increases. In this case, the soliton wave formed by the higher voltage overtakes the wave produced by the lower voltage, and then the oscillating soliton is formed in the final section of the line. The phase velocity can be calculated using [14]

$$\upsilon_p = 1/\sqrt{LC(V)} \qquad (1)$$

where C(V) is the variable capacitance as a function of the voltage applied across the varactor diode and L is the inductance.

The cutoff frequency of the line, known as the Bragg frequency, is given by [14]

$$f_c = 1/\pi\sqrt{LC(V_{max})} \qquad (2)$$

where C(Vmax) is the capacitance at the maximum voltage applied across the varactor diode.

Another important parameter of the line is the characteristic impedance [14]

$$Z_0 = \sqrt{L/C(V)} . \qquad (3)$$

The impedance of the line also depends on the reverse voltage applied on the diode varactor. As reported before the diode capacitance decreases with the voltage.

III. EXPERIMENTAL AND SIMULATION RESULTS

The measurements were performed on a 20-section capacitive NLTL that was built with linear inductors of 100 nH and SVC236 varactor diodes (Fig. 2).
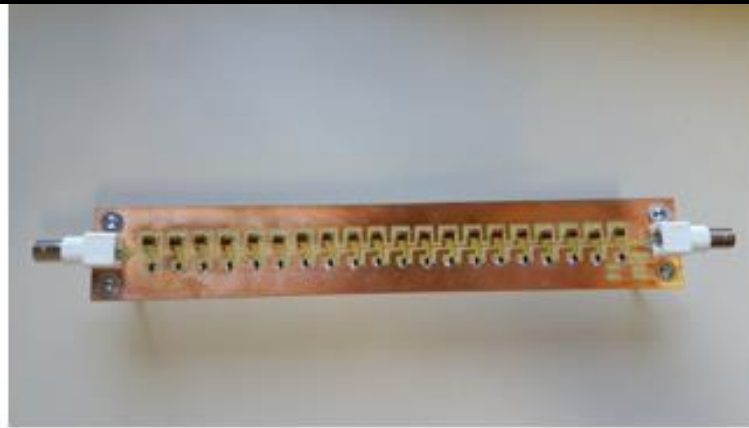
Fig. 2: Photograph of the 20-section capacitive NLTL.

The SVC236 diode capacitance-voltage behavior obtained from the manufacturer's datasheet [15] is shown in Fig. 3.
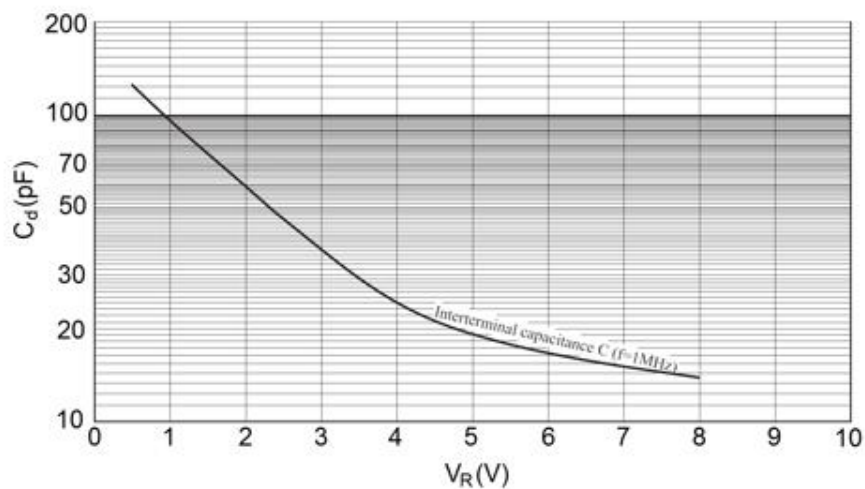

Fig. 3: Diode capacitance (C_d) as a function of reverse voltage (V_R).

From Fig. 3, making an extrapolation of the curve one obtains that $C(V_0)$ is of the order of 155 pF and $C(V_{max})$ is of about 11.5 pF, which gives 93% of capacitance change from the unbiased value to the capacitance value at 10 V.

Since the NLTL never fully matches the load as the line characteristic impedance according to (3) varies from an unstressed value of 93 Ω to a stressed value of 25 Ω, a resistive load of 50 Ω was used during the measurements at the output of the line and a pair of antenna with 50 Ω impedance was also used for radiation measurements.

The capacitive NLTL was driven by a function generator (HP 33120A) and a voltage amplifier (Apex PA98). It was supplied an input voltage of 13 V peak. A digital oscilloscope (Rohde & Schwarz RTE 1052) was used to perform the measurements.

3.1. LT-SPICE MODEL

The simulations were performed using the LT-SPICE software. The schematic circuit with 20 sections used for the simulations of the line directly connected to a resistive load and to a high-pass filter is shown in Figs. 4 and 5, respectively. In these models, the Ohmic losses (R_L=0.3 Ω and R_D=1.0 Ω) and the self-stray capacitance of the inductors (C_P=1.5 pF) were also considered. The simulation results were compared with the corresponding experimental results.
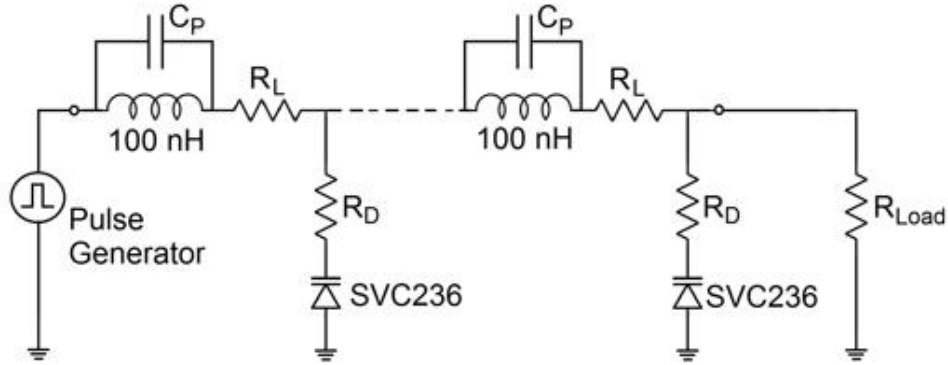
Fig. 4: NLTL schematic circuit model for the LT-SPICE simulations.
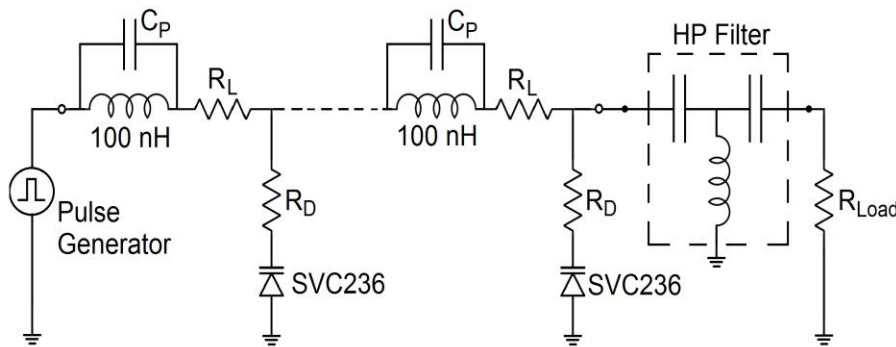

Fig. 5: NLTL schematic circuit model for the LT-SPICE simulations with the high-pass filter.

3.2. RESISTIVE LOAD MEASUREMENTS

The measurements were evaluated from the signal measured through the 50 Ω input of the oscilloscope. A 30 dB attenuator was connected between the line output and the oscilloscope input (Figs. 6 and 7).

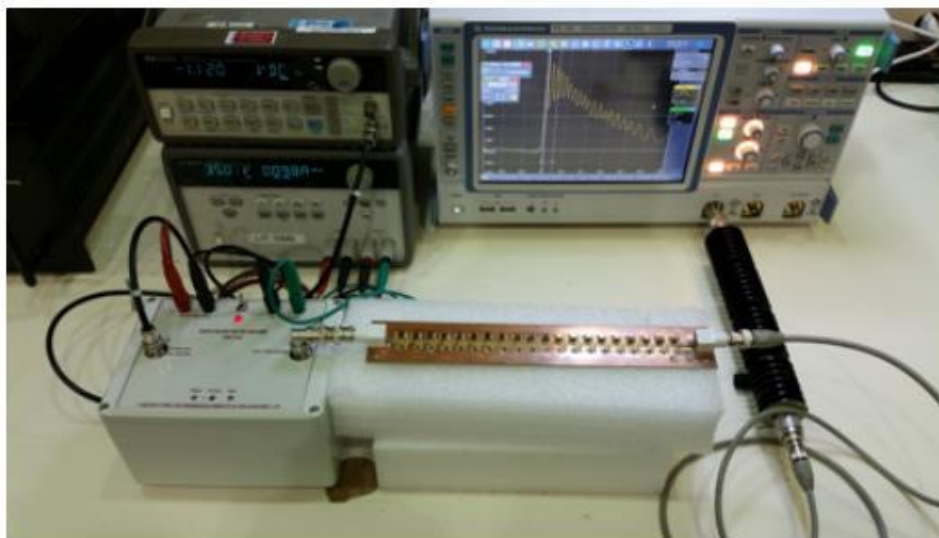*Fig. 6: Block diagram of the experiment with the 50 Ω load.*

Fig. 7: Photograph of the test setup.

The time response of the simulation and experimental measurement at the 50 Ω resistive load, according to the test setup shown in Fig. 6, is presented in Fig. 8 in short-time and long-time scales to show the pulse repetition frequency of 5 MHz.
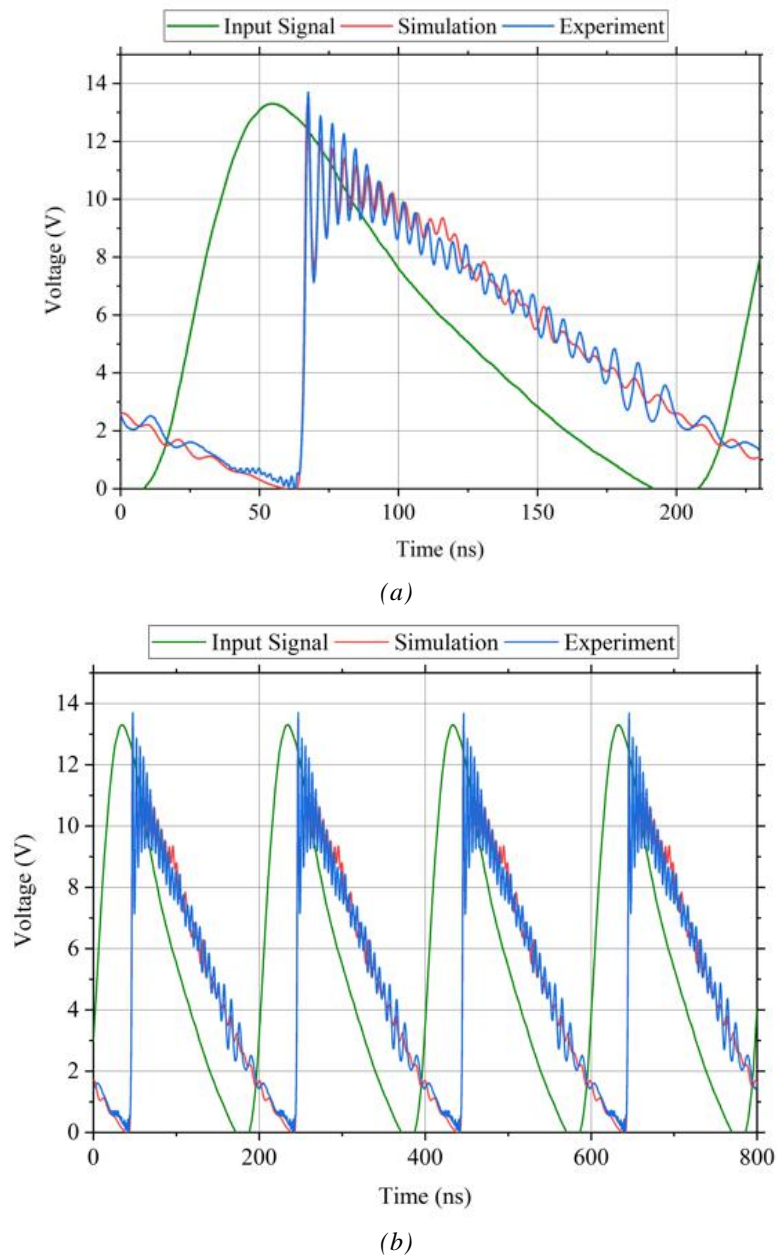

(a)

(b)

Fig. 8: Time domain plots of the input pulse (experimental) and the waveforms obtained on the 50 Ω resistive load (simulation and measurement) in a short-time scale (a) and in a long-time scale (b).

The frequency domain plot on the decibel scale is shown in Fig. 9. The frequency of the oscillations obtained from measurement and simulation is around 230 MHz.
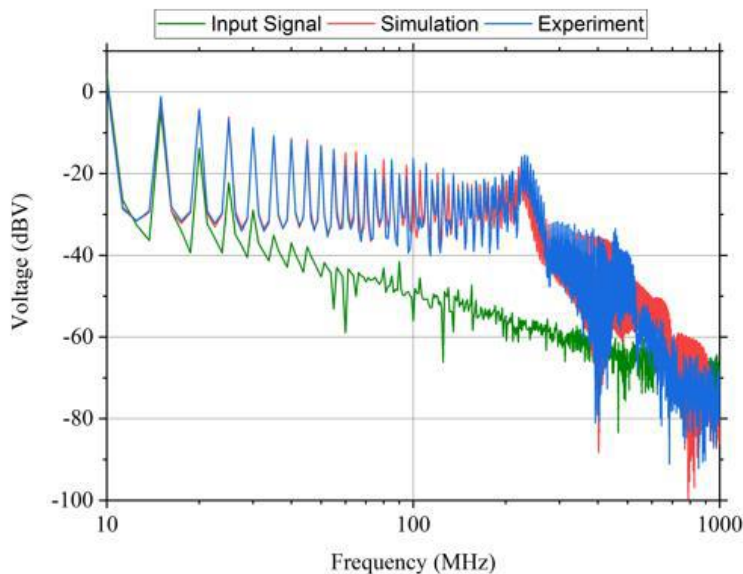
Fig. 9: FFT plot of the input pulse (experimental) and the pulsed RF signal (simulation and measurement) at the 50 Ω resistive load.

3.3. HIGH-PASS FILTER DESING AND MEASUREMENTS

According to Fig. 9, frequency component around 230 MHz was generated by the capacitive NLTL. In order to separate this frequency from the low voltage components of the input pulse signal, a high-pass filter with a cutoff frequency of 200 MHz was designed and connected at the output of the line. A third-order Chebyshev high-pass filter with T topology was chosen for this experiment. The Chebyshev response has ripples in the passband. For this experiment, 0.25 dB ripple was chosen as a designed parameter. Considering the line impedance equal to load impedance, the element values (C_1', L' and C_2') for a normalized Chebyshev filter with 0.25 dB ripple are 1.3034, 1.1463 and 1.3034, respectively [16]. The filter components were calculated according to [17,18]

$$C_1 = C_2 = 1/2\pi f C' Z_0 = 12.21 \ pF \qquad (4)$$

$$L = Z_0/2\pi f L' = 34.71 \ nH \qquad (5)$$

where L is the shunt inductor, C_1 and C_2 are the series capacitors connected to the line and the load, respectively, C'=C_1'=C_2'=1.3034 and L'=1.1463 are the normalized component values for the Chebyshev filter, $Z_0 = 50 \ \Omega$ and f = 200 MHz.

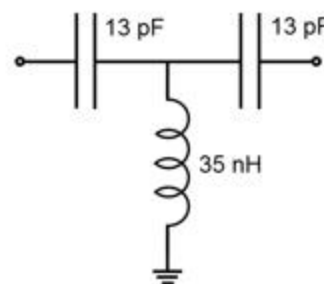The circuit was implemented using a commercial standard capacitor and inductor values (Fig. 10).

Fig. 10: High-pass 3rd order Chebyshev filter.

The filter was constructed in a separated circuit board to be characterized before the connection with the line (Fig. 11).

Fig.11: Filter photograph.

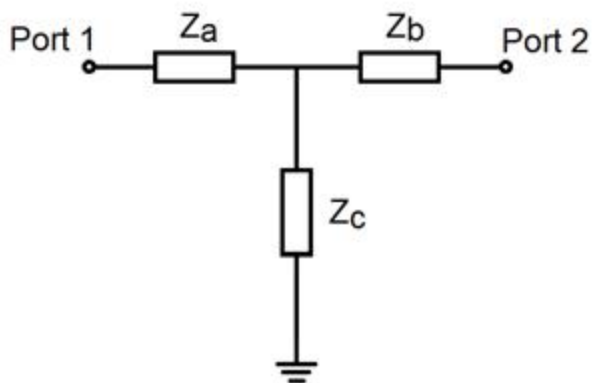For insertion loss calculation the filter circuit is represented by impedances (Fig. 12).

Fig. 12: Open-circuit impedances structure.

The network between port 1 and port 2 can be represented with the ABCD matrix as:

$$\begin{bmatrix} A & B \\ C & D \end{bmatrix} = \begin{bmatrix} 1 & Z_a \\ 0 & 1 \end{bmatrix} \cdot \begin{bmatrix} 1 & 0 \\ 1/Z_c & 1 \end{bmatrix} \cdot \begin{bmatrix} 1 & Z_b \\ 0 & 1 \end{bmatrix} \quad (6)$$

The impedances Z_a, Z_b, and Z_c can be calculated by

$$Z_a = -1/j\omega C_1 \quad (7)$$

$$Z_b = -1/j\omega C_2 \quad (8)$$

$$Z_c = j\omega L \quad (9)$$

where $C_1 = C_2 = 13$ pF, $L = 35$ nH and $\omega = 2\pi f$.

Then the elements of the ABCD matrix were calculated below

$$A = 1 + Z_a/Z_c \quad (10)$$

$$B = Z_a + Z_b + (Z_a Z_b/Z_c) \quad (11)$$

$$C = 1/Z_c \quad (12)$$

$$D = 1 + Z_b/Z_c \quad (13)$$

The relation between the input voltage (V_1) and current (I_1) and output voltage (V_2) and current (I_2) of a two-port network (Fig. 13) can be represented as:

$$\begin{bmatrix} V_1 \\ I_1 \end{bmatrix} = \begin{bmatrix} A & B \\ C & D \end{bmatrix} \begin{bmatrix} V_2 \\ -I_2 \end{bmatrix} \quad (14)$$

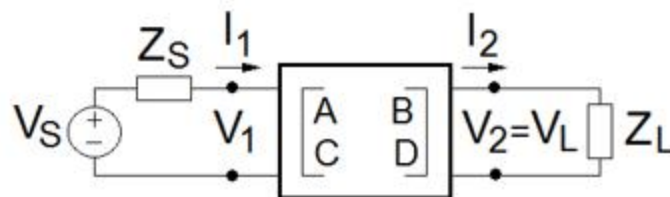where A, B, C, and D coefficients are frequency dependent.

Fig. 13: Two-port network.

The transfer function V_S/V_L for the circuit in Fig. 13 is given by

$$\frac{V_S}{V_L} = \frac{A Z_L + B + C Z_S Z_L + D Z_S}{Z_L} \quad (15)$$

where V_S and V_L are the source and load voltages, respectively, and Z_S and Z_L are source and load impedances, respectively.

Then, using (7)-(9), (10)-(13), and the ratio V_S/V_L given by (15), the insertion loss function can be calculated by

$$\frac{P_1}{P_2} = \left(\frac{Z_L}{Z_S + Z_L}\right)^2 \left|\frac{V_S}{V_L}\right|^2 \quad (16)$$

where P_1 is the power delivered to the load when the network is removed from the circuit whereas P_2 is the power delivered to the load when the network is in place.

Finally, the insertion loss (IL) of the filter can be expressed in dB:

$$IL = 10 \log\left(\frac{P_1}{P_2}\right) \ (dB). \quad (17)$$

Considering $Z_S = Z_L = 50 \ \Omega$ the insertion loss was calculated and measured through a Vector Network Analyzer (VNA) for the frequency range between 10 MHz and 500 MHz (Fig. 14).
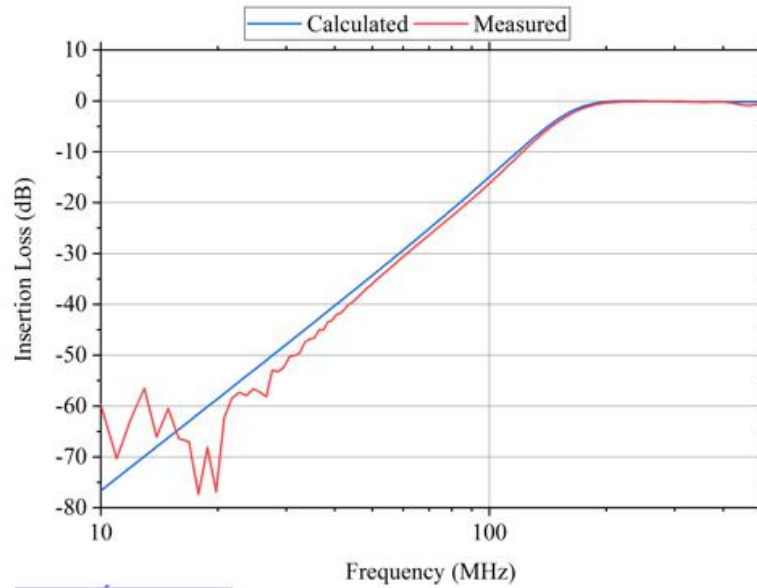
Fig. 14: Filter Insertion loss.

According to Fig. 14 the calculated insertion loss presents a good agreement with the measurement results.

The high-pass filter was connected to the output of the capacitive NLTL. The measurements were evaluated from the signal measured through the 50 Ω input of the oscilloscope (Fig. 15).
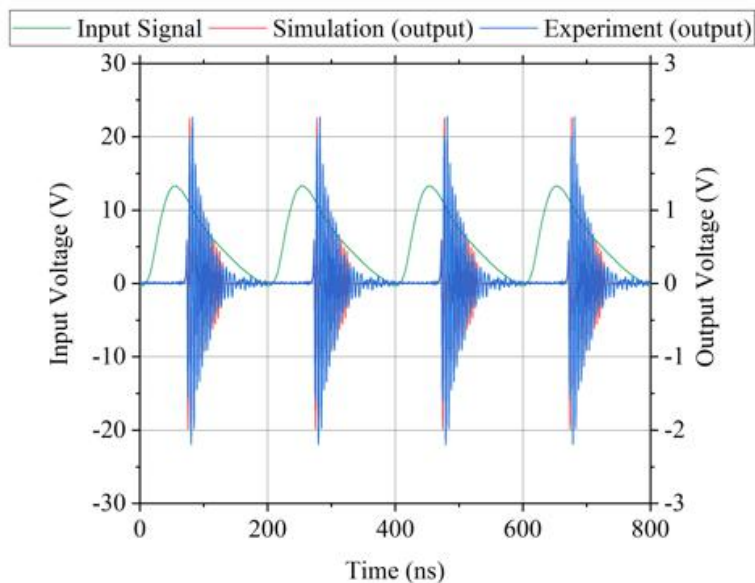

Fig. 15: Block diagram of the experiment with the high-pass filter.

The time response of the simulation and experimental measurement at the NLTL connected to a 50 Ω load through a high-pass filter, according to the test setup shown in Fig. 15, is presented in Fig. 16 in short-time and long-time scales. The frequency domain plot on the decibel scale is shown in Fig. 17.
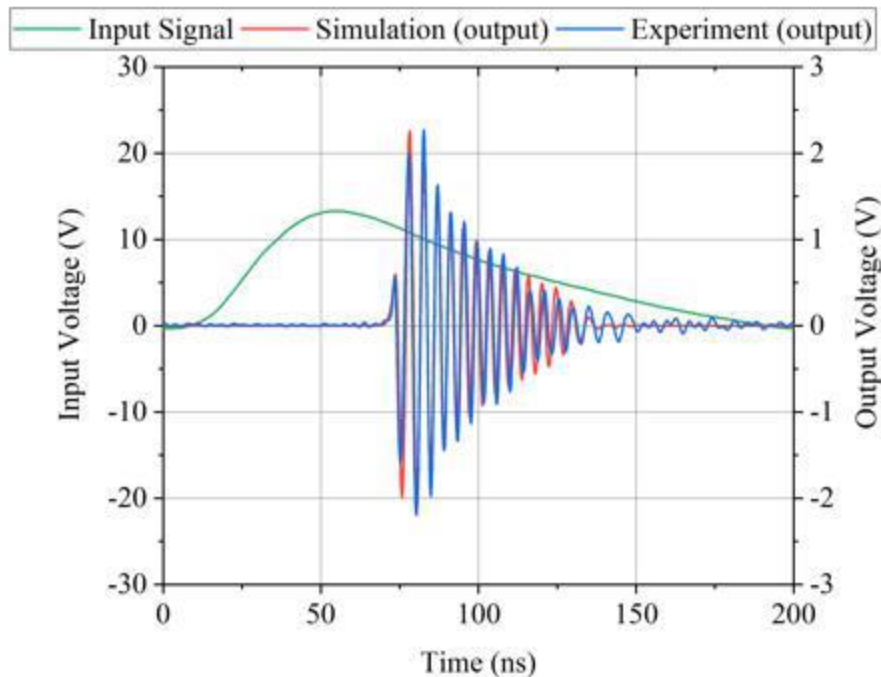
(a)

(b)

Fig. 16: Time domain plots of the input pulse (experimental) and the waveforms obtained on the 50 Ω resistive load (simulation and measurement) in a short-time scale (a) and in a long-time scale (b).
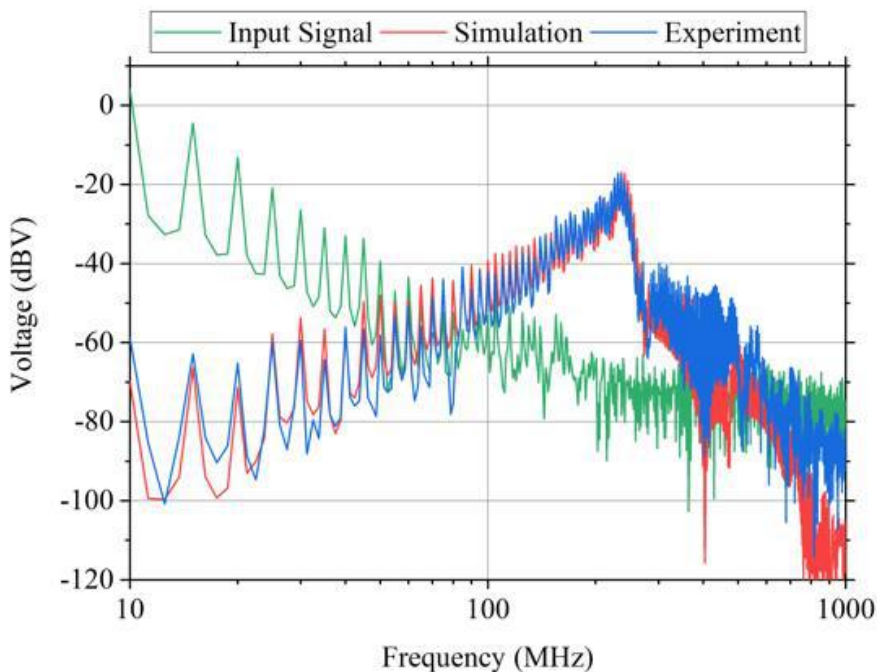

Fig. 17: FFT plot of the input pulse (experimental) and measured on the 50 Ω resistive load when the filter is connected to the line (simulation and measurement.

Fig. 18 shows the comparison between the measurements of the RF pulsed signal at the output of the line without the high-pass filter (Fig. 9) and with the high-pass filter (Fig. 17). It is possible to see that the filter provided a high attenuation for the low-frequency components.
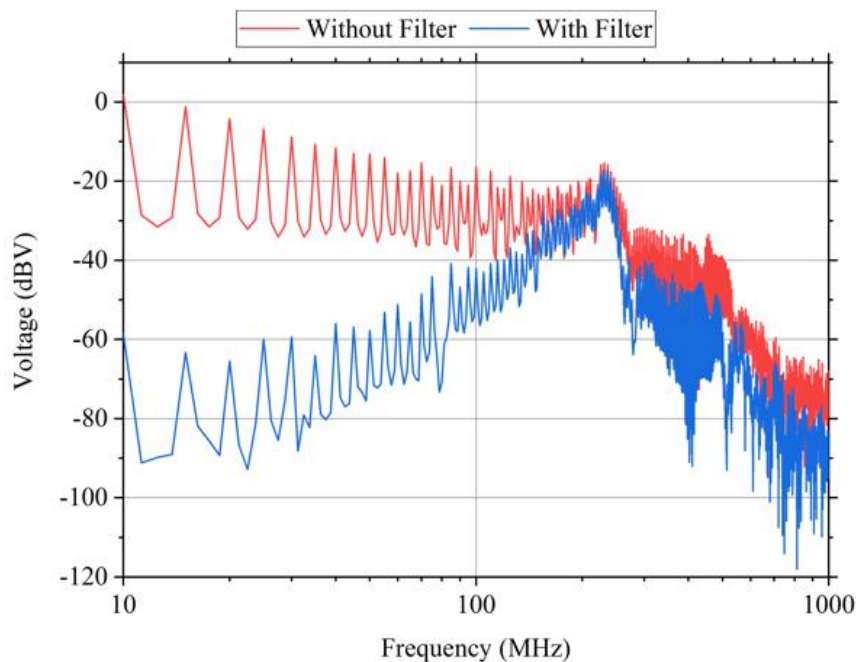
Fig. 18: FFT plot of the pulsed RF signal measured at the 50 Ω with and without the high-pass filter.

IV.   RADIATION MEASUREMENTS

Two Double-Ridged Guide (DRG) antennas (ETS-Lindgren 3106B) were used to transmit and receive the RF signal. It is a broadband antenna that operates in the frequency band from 200 MHz up to 1 GHz.

The antennas were placed in vertical polarization with a two-meter spacing. The receiving antenna terminal was connected through a coaxial cable to the 50 Ω input of the oscilloscope.

The measurements were performed in an anechoic chamber to avoid electromagnetic interference (Figs. 19 and 20).
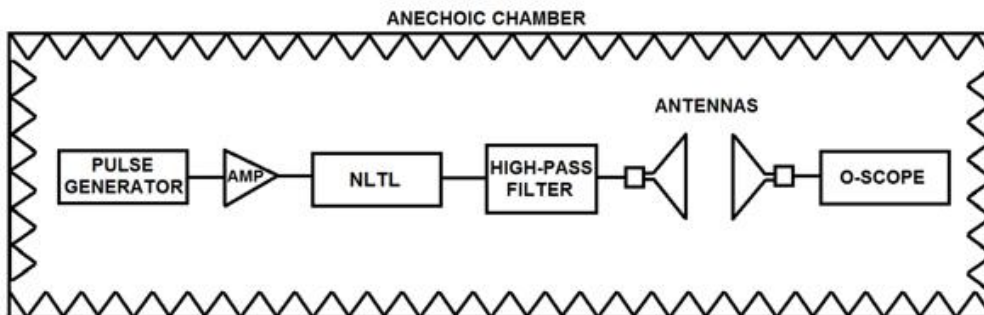

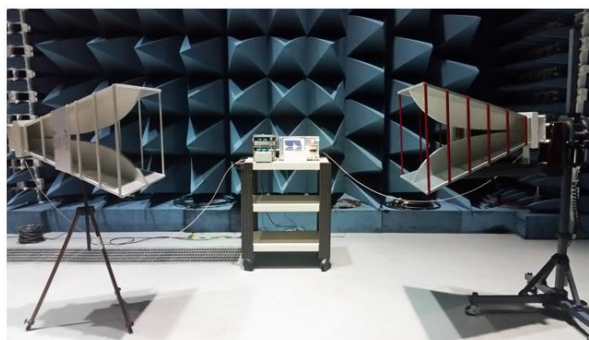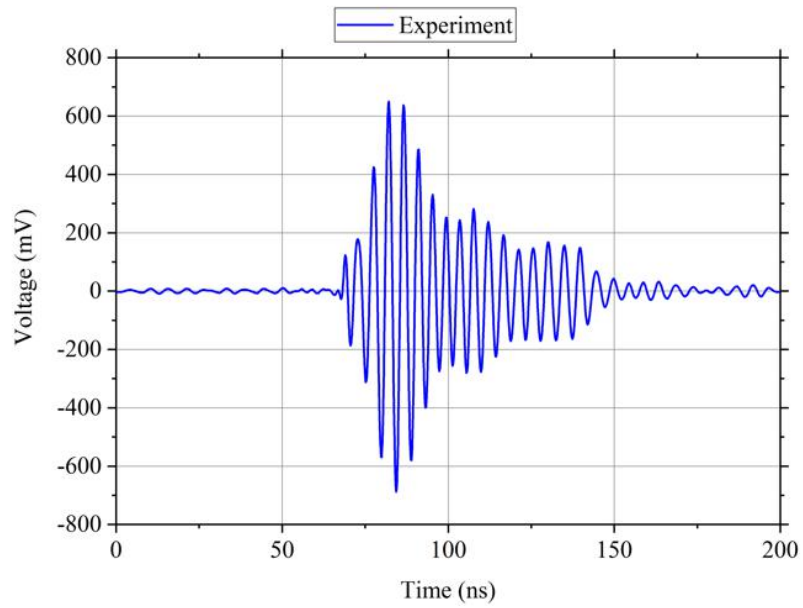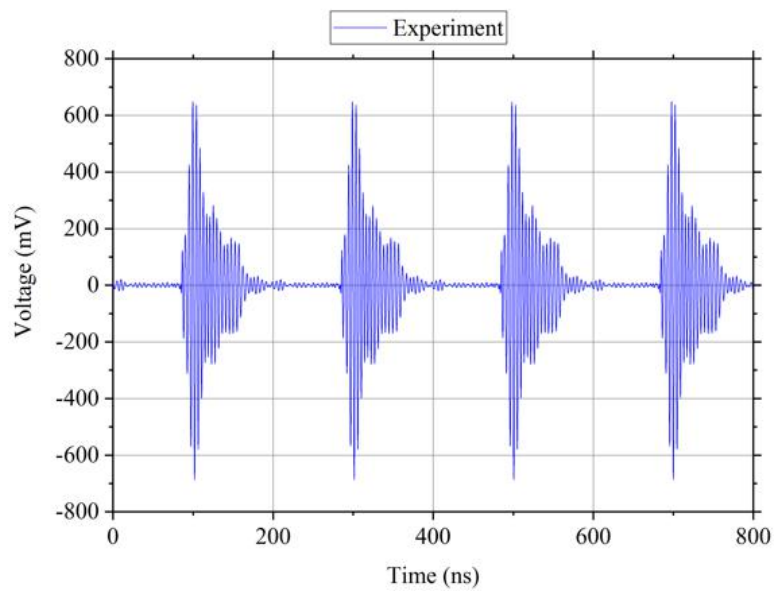*Fig. 19: Block diagram of the experiment with DRG antennas.*

Fig. 20: Photograph of the test setup in the anechoic chamber.

The time response of the RF signal measurement captured by the receiving antenna, according to the test setup shown in Fig. 19, is presented in Fig. 21 in short-time and long-time scales. The frequency domain plot is shown in Fig. 22.

(a)

(b)

Fig. 21: Time domain plots of the signal received by the DRG antenna in a short-time scale (a) and in a long-time scale (b).
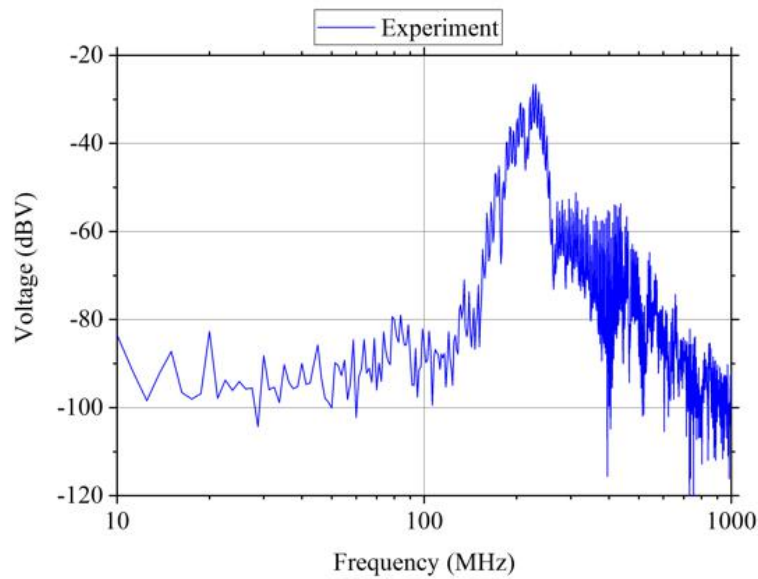
Fig. 22: FFT plot of the pulsed RF signal received by the DRG antenna.

Fig. 23 shows the comparison between the RF pulsed signal at the output of the line without the high-pass filter (Fig. 9), with the high-pass filter (Fig. 17) and received by the DRG antenna (Fig. 22).
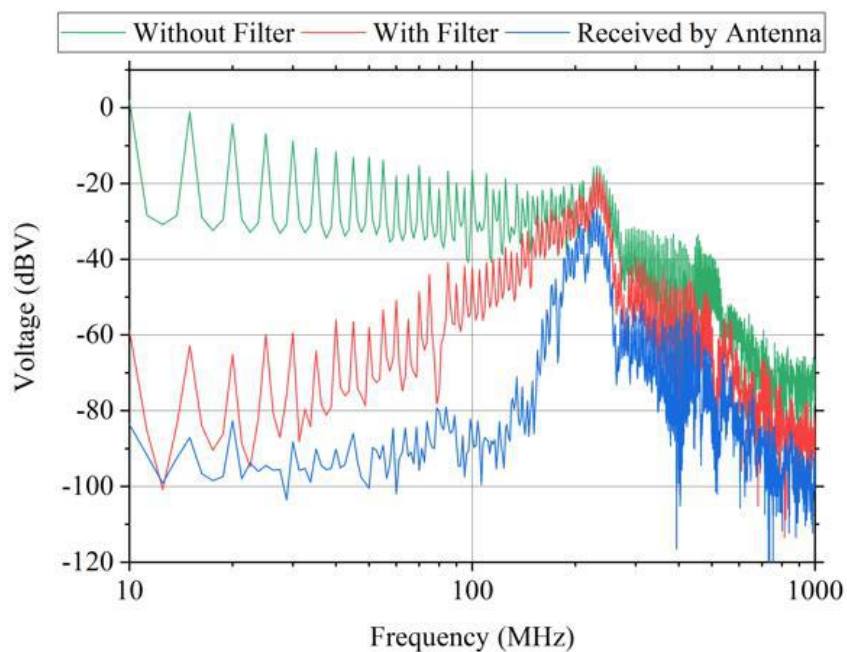

Fig. 23: FFT plot of the pulsed RF signal measured at the 50 Ω load with and without the filter and received by the DRG antenna.

V.   CONCLUSION

This article reports the excellent results obtained with a 20-section low voltage lumped capacitive NLTL in which oscillations of the order of 230 MHz were produced and radiated using Double-Ridged Guide (DRG) antennas. The performance of the line was investigated focusing on the extracting of the RF signal from the line and the irradiation by an antenna.

The LT-SPICE models implemented for simulations presented a good agreement with the experimental data.

It was demonstrated that the Chebyshev filter is very efficient in extracting the RF signal from the soliton pulse. The insertion loss is less than 1 dB within its passband and it provided a 60 dB attenuation for the lower frequency components. The oscillation frequency remains practically the same around 230 MHz for the three different cases:

- Measurement of the signals performed directly at the 50 Ω load;

- Measurement of the RF signals extracted from the line through a high-pass filter;

- Measurement of the RF signals received by an antenna.

The RF pulses have been perfectly transmitted and received by the DRG antenna. Future work shall include the analysis of different filter topologies for the decoupling circuit.

ACKNOWLEDGEMENTS

REFERENCES

[1] J. D. Darling and P. W. Smith, "High power pulse burst generation by soliton-type oscillation on nonlinear lumped element transmission lines," in *Proc. 2009 IEEE Int. Pulsed Power Conference*, Washington, DC, 2009, pp. 119-123.

[2] J. O. Rossi, L. P. S. Neto, F. S. Yamasaki, and J. J. Barroso, "State of the Art of Nonlinear Transmission Lines for Applications in High Power Microwaves," in *2013 SBMO/IEEE MTT-S*, Rio de Janeiro, pp. 1-5.

[3] N. Seddon, C. R. Spikings, and J. E. Dolan, "RF pulse formation in nonlinear transmission lines," in *Proc. 2007 IEEE Int. Pulsed Power Conf.*, Albuquerque, NM, pp. 678-681.

[4] M. P. Brown and P. W. Smith, "High power, pulsed soliton generation at radio and microwave frequencies," in Proc. 11th IEEE Int. Pulsed Power Conf., Jun. 1997, pp. 346–354.

[5] D. Yoshida, H. Ishizawa, T. Tanabe, K. Sugimoto, S.H.R. Hosseini, S. Katsuki, and H. Akiyama, "Development of burst high frequency wave source for medical application," in *Proc. 2013 19th IEEE Int. Pulsed Power Conf., (PPC)*, San Francisco, CA, 2013, pp. 1-4.

[6] K. Yasu, Y. Minamitani, and K. Nukaga, "Development of high-power burst pulse generator based on magnetic switch for bioelectrics application," in *Proc. 2016 IEEE International Power Modulator and High Voltage Conference (IPMHVC)*, San Francisco, CA, 2016, pp. 392-396.

[7] S. Mondal, M. I. M. Ghazali, S. Karuppuswami, A. Kaur, and P. Chahal, "A nonlinear transmission line based harmonic RF tag," in *Proc. 2017 IEEE 67th Electronic Components and Technology Conference (ECTC)*, Orlando, FL, 2017, pp. 2237-2242.

[8] X. Jia, Q. Feng, T. Fan, and Q. Lei, "RFID technology and its applications in Internet of Things (IoT)," in *Proc. 2012 2nd International Conference on Consumer Electronics, Communications and Networks (CECNet)*, Yichang, China, 2012, pp. 1282-1285.

[9] A. Moreira, P. Prats-Iraola, M. Younis, G. Krieger, I. Hajnsek, and K. P. Papathanassiou, "A tutorial on synthetic aperture radar," in *IEEE Geosci. Remote Sens.*, vol. 1, no. 1, pp. 6-43, March 2013.

[10] E. Peral, E. Im, L. Wye, S. Lee, S. Tanelli, Y. Rahmat-Samii, S. Horst, J. Hoffman, S. Yun, T. Imken, and D. Hawkins, "Radar technologies for earth remote sensing from cubesat platforms," *Proceedings of the IEEE*, Vol. 106, Issue 3, March 2018, pp. 404-418.

[11] M. S. Nikoo and S. M. Hashemi, "New soliton of a varactor-loaded nonlinear transmission line," IEEE Trans. on Microwave Theory and Techniques, vol. 65, no 11, pp. 4084-4092, Nov. 2017.

[12] E. G. L. Rangel, J. J. Barroso, J. O. Rossi, F. S. Yamasaki, L. P. Silva Neto, and E. Schamiloglu, "Influence of input pulse shape on RF generation in nonlinear transmission lines," *IEEE Trans. Plasma Sci.*, vol. 44, no. 10, pp. 2258-2267, Oct. 2016.

[13] L. P. S. Neto, J. O. Rossi, J. J. Barroso, and F. S. Yamasaki, "RF pulse formation in NLTLs using varactor diode," *in Proc. Symp. Oper. Appl. Areas of Defense (SIGE)*, S. J. Campos, 2014, pp. 43-48.

[14] P. W. Smith, "Nonlinear Pulsed Power" in *Transient electronics – Pulsed Circuit Technology*, John Wiley & Sons, West Sussex, England, 2002, Ch. 8, pp. 247.

[15] Semiconductor Components Industries, LLC, "SVC236 datasheet, monolithic dual varactor diode for FM tuning," pp. 1-6, September 2013.

[16] L. Weinberg, "Additional tables for design of optimum ladder networks," *in Journal of the Franklin Institute,* Volume 264, Issue 1, July 1957, Pages 7-23.

[17] S. Winder, *Analog and Digital Filter Design*, 2nd edition, Newnes, USA, 2002.

[18] G. L. Matthaei, L. Young, and E. M. Jones, *Design of Microwave Filters, Impedance-Matching Networks, and Coupling Structures*, Volume 1, DTIC Document, 1963.